MRI-Guided Optical Tomography:

Prospects and Computation for a New Imaging Method

Randall L. Barbour, Harry L. Graber, and Jenghwa Chang
SUNY Health Science Center at Brooklyn

San-Lian S. Barbour, Ping C. Koo, and Raphael Aronson
Bioimaging Sciences Corporation

Living tissue scatters near-infrared light randomly. Can this problem be overcome to make NIR optical tomography possible? If so, it could be more accurate and less damaging than other medical imaging techniques. Computational experiments using combined MRI–optical methods show promise.

Many people, perhaps as children, have seen the red glow produced by placing a flashlight to the palm of a hand or inside the mouth. This simple experiment teaches us that red light can penetrate through relatively thick tissues. At near-infrared (NIR) wavelengths (about 700 to 1,300 nm), even greater penetration is possible. As far back as 1929, investigators recognized the potential of employing NIR optical measurements for the study of tissues.[1]

Since that time computers, combined with advances in the mathematics and algorithmics of inverse problems, have made it possible to use various frequencies of electromagnetic (and other) energy for much more sophisticated methods of medical imaging. For example, X rays are now routinely used not only to create the commonly recognized two-dimensional images on film, but to produce cross-sectional digital images of the body that can be built up into a true 3D composite. This technique, known as tomography (or computed tomography, whence *CT scan*) creates an image by computational analysis of multiple measurements made from different directions surrounding an object. Of special interest would be to somehow use optical measurements in a similar manner.

There are many potential benefits to doing this. Unlike X rays, NIR photons do not cause tissue damage. Measurements can be performed with great sensitivity and, in many cases, can employ relatively low-cost, compact instrumentation. The obvious difficulty is that despite significant penetration at these wavelengths, tissues appear opaque because of the intense scattering experienced by the migrating photons. Until quite recently, many would have argued (and some still do) that this spells certain doom for any hope of recovering usable images.

At the heart of the matter is whether it is possible to produce an image of the interior of a random-scattering medium. Conventional wisdom would argue that if there is no well-defined path for the signal propagating from a source to a detector, there is no possibility of recovering an image.[2] This position is not without intuitive merit: the mythological Theseus was able to find his way out of the Labyrinth by following a piece of string he'd laid down

1070-9924/95/$4.00 © 1995 IEEE

while entering it, but it is easy to see that the "strings" corresponding to individual NIR photon trajectories in thick tissue structures are thoroughly tied in knots. Why should it be possible to disentangle this mass of threads? In this article we describe strategies we are pursuing to do this, and some recent findings. We hope they will convince even the most hardened skeptic that this problem is *not* hopeless. On the contrary, there is reason for optimism that practical systems can be developed.

Any problem worth studying must have some basic irresistible features. Ours has two. First, we recognize that scattering of penetrating or emitted energy severely limits the achievable resolution in many types of imaging problems. Extracting useful information from scattering measurements could greatly extend the depth or thickness of media that could be explored and the types of energy sources that could be employed. Many fields have imaging problems that are made more difficult by scattering—geophysics, materials testing, surveillance, and medicine, for instance—and image enhancement strategies applicable to any one of these could prove useful to all. This has caught the attention of many researchers. The second reason we find the problem irresistible is the breadth of potential applications to clinical medicine. Several physiologically important pigments can easily be studied at NIR wavelengths; in particular, hemoglobin. Measurement of the oxygen-dependent spectral changes of hemoglobin, which are closely linked to tissue function, has significant practical value, especially for detecting serious medical problems such as strokes or hemorrhages. Optical methods also are well suited for the study of dynamic events. Such measurements could be of particular value in the monitoring of brain function.

From electromagnetic theory, we learn that solutions to the inverse scattering problem (see sidebar) can be obtained from formulations derived from Maxwell's equations. This approach is the foundation for diffraction tomography, which has been successfully applied to acoustic and microwave imaging. While formulations based on electromagnetic theory can be applied to the optical tomography problem, the much more intense scattering of photons in tissue quickly renders any serious examination of such data intractable. An alternative formulation, also capable of accounting for the effects of scattering, is *transport theory*, which treats propagating photons as particles. This is a valid simplification if the phases of the various contributions to the net scattered field are uncorrelated, a condition satisfied in almost all cases of thick tissues illuminated by NIR light. The chief advantage of the transport theory approach is that it brings relative computational simplicity to a complex physical phenomenon.

Several years ago, some of us[3,4] described an image-recovery scheme derived from transport theory that is suitable for examining the interior properties of opaque, dense scattering media. Independently, others[5,6] have described alternative schemes formulated upon random-walk and diffusion theories. Our approaches and those of Arridge et al. consider a tomographic-type measurement scheme, similar to that commonly employed in other imaging modalities, and entail solving a system of linear equations that computes the difference in optical coefficients between the unknown medium and a defined reference medium. In physics, this is commonly referred to as solving a linear perturbation problem.

The principal difference between this method and, for example, X-ray computed tomography, is that we use imaging operators that explicitly take into account the effects of multiple scattering. The physical interpretation of these operators is that each one represents the spatial probability distribution of photons launched from a source that enter a specified detector. A map of this distribution is similar to a cloud. It has fuzzy borders, with some regions more dense than others. The regions of greatest importance usually lie near the source and detector. Factors that determine the shape of this distribution are defined by parameters that specify the forward problem. These include the optical coefficients of the medium, that is, the absorption and scattering cross sections; the medium's shape; and properties of the source and detector, in particular the temporal resolution of measurement.

Improvements in data collection and analysis: Development of modeling strategies

Much of the ongoing effort in this field is directed toward developing improved algorithms and appropriate data collection schemes. The latter refers to refinement of the physical measurement (number of optical sources and detectors, view angle, etc.) and whether other types of data may be required to compute an optical image. Such efforts

Inverse Problems, Forward Problems

Two terms commonly used in describing imaging problems are the *inverse problem* and the *forward problem*. The inverse problem is one in the form of: Given a set of measured responses, determine the internal properties of the medium. That is, the inverse problem is the process of actually computing the image. In a forward problem, one seeks to determine the properties of the emerging signal (such as intensity) that would be expected in a given measurement for a specified set of input conditions. Solutions to the forward problem are often used to predict expected sensitivities of a measurement.

invariably require the weighing of trade-offs between practical measurements and a tractable computation. One of our goals has been to devise a procedure incorporating anatomically accurate models of tissues that is well suited to systematically exploring these trade-offs. In particular, we are using magnetic resonance–derived data because of its high resolution and excellent contrast of soft tissues, and because 3D anatomical information can be easily obtained. We do so both for the purpose of method refinement and to explore the feasibility of acquiring optical measurements simultaneously with MRI. In this context, the phrase "MRI-guided optical tomography" has a dual meaning. Further, we adopt the modeling of anatomically accurate media because of the expected sensitivity of the trade-offs to the structure of the media.

Use of imaging data from one modality to aid in the development and application of another is becoming increasingly popular, in part due to improved methods for image segmentation and registration. The MR method as a means of acquiring a priori anatomical information has added significance for optical tomography because of the apparent practicality of acquiring simultaneous optical and MR measurements. In practice, this would require use of optical fibers to deliver light to the tissue and to transmit emitted light to detectors positioned at a sufficient distance from the magnet so as not to be affected by the magnetic field. While the breadth of MR applications continues to grow, the merits of a combined MR–optical measurement are undiminished. Optical methods are orders of magnitude more sensitive than MRI, especially when fluorescence measurements are made, and are sensitive to different physical parameters. Thus, it would appear that there are strong elements of synergism associated with combining MR and optical tomographic methods.

In the following, we present a brief description of the perturbation model and some details of numerical experiments we have conducted using MR-derived data sets. We believe that this modeling scheme is an efficient and cost-effective means to systematically explore the merits of various strategies for collecting optical data to use with a variety of algorithms. We have numerically simulated a range of optical tomographic measurements to explore how best to acquire and analyze data. Specifically, we simulated detector readings for a variety of source–detector pairs for a breast with and without assumed defined inclusions. The calculations of light diffusion were simulated. The optical data for the "medium," the breast, were obtained by assigning an assumed set of optical coefficients for each type of breast tissue as determined by segmentation of an actual MR image of the breast. The model was highly simplified and is discussed in detail below.

Important factors we explored include the geometry of the illumination scheme, the source condition, the number and location of sources and detectors, and the influence of systematic and random errors that degrade image quality. Our basic method involves computing solutions to the forward problem for segmented 3D MR data sets in which the identified tissue types have been assigned optical coefficients. In this manner we can easily simulate a tomographic measurement using a model that is anatomically accurate, and for which we can vary the contrast, size, and number of simulated pathologies in relation to a range of properties of the background tissue. For any particular tomographic data set we can also explore the dependence of image quality on issues related to the implementation of an algorithm, such as use of range constraints, regularization methods, and the effects of ill-conditioning and ill-posedness. Thus, our approach is well suited for optimizing data collection and data analysis schemes while at the same time providing insight into the utility of acquiring simultaneous MR and optical data inside an MR magnet.

Formulation of the imaging problem

The governing equation describing the migration of photons that experience elastic scattering, under the assumption that it is appropriate to treat photons as Newtonian particles, is the one-speed radiation transport equation. This is an integro-differential balance equation each of whose terms accounts for one of the physical processes that influence the angular intensity distribution within a specified medium. In the limit of weak absorption, weakly anisotropic scattering, and coefficients that vary only slowly in the spatial domain, solutions to the diffusion equation are excellent approximations to those of the transport equation. The continuous diffusion equation with inhomogeneous diffusion constant $D(\mathbf{r})$ is

$$\frac{1}{c_n}\frac{\partial}{\partial t}\Phi(\mathbf{r},t) - \nabla\cdot[D(\mathbf{r})\nabla\Phi(\mathbf{r},t)] + \mu_a(\mathbf{r})\Phi(\mathbf{r},t) = S(\mathbf{r},t) \quad (1)$$

where $\Phi(\mathbf{r}, t)$ [measured in $cm^{-2}\ s^{-1}$] is the diffuse intensity at position $\mathbf{r}$ and time t, $S(\mathbf{r}, t)$ [$cm^{-3}\ s^{-1}$] is the source strength at position $\mathbf{r}$ and time t, $\mu_a(\mathbf{r})$ [cm^{-1}] is the position-dependent absorption coefficient, $D(\mathbf{r})$ [cm] is the position-dependent diffusion coefficient, and c_n is the speed of light in the medium. $D(\mathbf{r})$ is related to the absorption and scattering coefficients by

$$D(\mathbf{r}) = \frac{1}{3\left[\mu_a(\mathbf{r}) + \mu_s(\mathbf{r})(1-g)\right]} = \frac{1}{3\left[\mu_a(\mathbf{r}) + \mu_s'(\mathbf{r})\right]}$$

where $\mu_s(\mathbf{r})$ [cm^{-1}] is the position-dependent scattering coefficient and g [dimensionless] is the scattering anisotropy parameter, equal to the average value of the cosine of the angle through which photons are scattered. For the product $\mu_s(\mathbf{r})(1-g)$ we will use the notation $\mu_s'(\mathbf{r})$ [cm^{-1}], which is known as the *reduced* scattering coefficient.

An important experimental control parameter is the time-dependence of $S(\mathbf{r}, t)$. Three source types have received particular attention. One set of investigators favors illuminating a target with trains of very brief pulses of light ($\Delta t < 1$ picosecond is readily achievable in practice) and measuring time-resolved detector responses. Another approach uses time-harmonic sources, in which the illumination is continuous but with an intensity that varies (at a rate of around 100 MHz to 1 GHz) about the mean level. The measured quantities at the detector in this case are the mean intensity or flux, the amplitude of its variation, and the phase of the detected light relative to the incident light. The impulse-response and time-harmonic approaches are a Fourier pair, so in theory the same information regarding the structure of a target medium is obtainable either way, and the choice usually hinges on practical considerations such as the comparative difficulties and costs of making and/or analyzing the measurements. The third approach is illumination of the medium with time-independent sources and measurement of the intensity or flux. This is the method we have used here. It has clear practical advantages in terms of simplifying the experimental or clinical collection of data, but the information content of the detector readings may be intrinsically lower. Note that the continuous-wave approach is a limiting case of both the time-resolved (long pulse duration limit) and time-harmonic (low frequency limit) domains.

Perturbation model

We have previously described a linear perturbation model, based on the transport equation, for imaging differences in the optical coefficients for an arbitrary medium.[3,4,7] The results described here use the *diffusion* equation to compute detector responses and the intensity of light in the interior of the target and reference media. Thus, the quantities that may be imaged are the perturbations of the absorption and diffusion coefficients, $\Delta\mu_a(\mathbf{r})$ and $\Delta D(\mathbf{r})$, of the target relative to the reference. Here we sketch the derivation of the appropriate continuous-wave perturbation model for diffusion.

The time-independent diffusion equation for the reference medium is

$$S(\mathbf{r}) + \nabla\cdot\left[D(\mathbf{r})\nabla\Phi(\mathbf{r})\right] - \mu_a(\mathbf{r})\Phi(\mathbf{r}) = 0 \qquad (2)$$

Assume that the position-dependent diffusion and absorption coefficients in the *target* medium are small perturbations to those in the reference medium. Then the light intensity distribution in the target is likewise equal to the reference intensity plus a perturbation:

$$S(\mathbf{r}) + \nabla\cdot\left\{\left[D(\mathbf{r}) + \Delta D(\mathbf{r})\right]\nabla\left[\Phi(\mathbf{r}) + \Delta\Phi(\mathbf{r})\right]\right\} - \left[\mu_a(\mathbf{r}) + \Delta\mu_a(\mathbf{r})\right]\left[\Phi(\mathbf{r}) + \Delta\Phi(\mathbf{r})\right] = 0 \qquad (3)$$

When we multiply out all terms in Equation 3 and then subtract Equation 2 from it, we are left with

$$\nabla\cdot\left\{D(\mathbf{r})\nabla\left[\Delta\Phi(\mathbf{r})\right] + \Delta D(\mathbf{r})\nabla\Phi(\mathbf{r}) + \Delta D(\mathbf{r})\nabla\left[\Delta\Phi(\mathbf{r})\right]\right\} - \mu_a(\mathbf{r})\Delta\Phi(\mathbf{r}) - \Delta\mu_a(\mathbf{r})\Phi(\mathbf{r}) - \Delta\mu_a(\mathbf{r})\Delta\Phi(\mathbf{r}) = 0 \qquad (4)$$

Our basic linearity assumption, which is valid for sufficiently small $\Delta\mu_a(\mathbf{r})$ and $\Delta D(\mathbf{r})$, is that the second-order perturbation terms in Equation 4 can be neglected, so that

$$\begin{aligned} 0 &\approx \nabla\cdot\left\{D(\mathbf{r})\nabla\left[\Delta\Phi(\mathbf{r})\right]\right\} - \mu_a(\mathbf{r})\Delta\Phi(\mathbf{r}) + \left\{\nabla\cdot\left[\Delta D(\mathbf{r})\nabla\Phi(\mathbf{r})\right] - \Delta\mu_a(\mathbf{r})\Phi(\mathbf{r})\right\} \\ &= \nabla\cdot\left\{D(\mathbf{r})\nabla\left[\Delta\Phi(\mathbf{r})\right]\right\} - \mu_a(\mathbf{r})\Delta\Phi(\mathbf{r}) + S'(\mathbf{r}) \end{aligned} \qquad (5)$$

Thus, the light intensity perturbation obeys a diffusion equation, in which the absorption and diffusion coefficient distributions are those of the *reference* medium. The problem of image reconstruction is mathematically equivalent to that of solving for the unknown source function $S'(\mathbf{r})$.

In the linear regime, the general expression for the difference in detector response, ΔR, between the target and reference media is

$$\Delta R = \int_V \left[w_a(\mathbf{r})\Delta\mu_a(\mathbf{r}) + w_D(\mathbf{r})\Delta D(\mathbf{r})\right] d^3\mathbf{r} \qquad (6)$$

where $w_a(\mathbf{r})$ and $w_D(\mathbf{r})$ are the appropriate *weight functions* for the absorption and diffusion coefficients at $\mathbf{r}$. Here,

$$w_a(\mathbf{r}) = -\Phi(\mathbf{r})\Phi^+(\mathbf{r}), \quad w_D(\mathbf{r}) = -\nabla\Phi(\mathbf{r})\cdot\nabla\Phi^+(\mathbf{r}) \qquad (7)$$

where $\Phi^+(\mathbf{r})$ denotes the *adjoint* intensity, which is defined as the detector response due to one photon born per second at $\mathbf{r}$ and emitted isotropically. It has a well-known alternate interpretation as the intensity at $\mathbf{r}$ due to one photon per second injected into the medium from the detector. Thus, the same methods used for computation of $\Phi(\mathbf{r})$ can also be used to compute $\Phi^+(\mathbf{r})$.

The absorption weight function is readily interpreted. The factor $\Delta\mu_a(\mathbf{r})\Phi(\mathbf{r})$ is the excess absorption rate in the linear approximation per unit volume at $\mathbf{r}$ due to $\Delta\mu_a(\mathbf{r})$. Thus $-\Delta\mu_a(\mathbf{r})\Phi(\mathbf{r})\Phi^+(\mathbf{r})d^3\mathbf{r}$ is the decrease in the intensity at the detector due to the extra absorptions in $d^3\mathbf{r}$. The expression for $w_D(\mathbf{r})$ is not as easily interpreted physically.

Let the target medium be discretized into $\mathcal{J}$ nonoverlapping voxels and let $\Delta\mu_{a,j}$ be the volume-averaged perturbation of the absorption coefficient in voxel j. Extension to changes in the diffusion coefficient is immediate. Let I be the total number of source–detector pairs and ΔR_i be the detector reading for the ith source–detector pair. Then Equation 6 can be recast as a system of linear equations

$$\Delta\mathbf{R} = W\Delta\boldsymbol{\mu}_a \tag{8}$$

where

$$\Delta\mathbf{R} = \begin{bmatrix} \Delta R_1 \\ \Delta R_2 \\ \vdots \\ \Delta R_I \end{bmatrix}, \quad W = \begin{bmatrix} w_{11} & w_{12} & \cdots & w_{1\mathcal{J}} \\ w_{21} & w_{22} & \cdots & w_{2\mathcal{J}} \\ \vdots & \vdots & \ddots & \vdots \\ w_{I1} & w_{I2} & \cdots & w_{I\mathcal{J}} \end{bmatrix}, \text{ and}$$

$$\Delta\boldsymbol{\mu}_a = \begin{bmatrix} \Delta\mu_{a,1} \\ \Delta\mu_{a,2} \\ \vdots \\ \Delta\mu_{a,\mathcal{J}} \end{bmatrix}.$$

Here, the matrix elements w_{ij} are the discrete analogs of the continuous weight function in Equation 7.

The inverse problem can also be stated as follows: given a set of source–detector pairs, the perturbed detector readings $\Delta\mathbf{R}$, and the precalculated weight function W, find the perturbation of the absorption coefficients $\Delta\boldsymbol{\mu}_a$ of the target medium.

Setting up the reference medium from MR data

The basic approach we use is to perform a series of MR measurements on the breast of a volunteer, segment the resulting images according to tissue type, assign estimates of the optical coefficients to the background tissues, and introduce "virtual tumors" to selected areas. The resulting data set becomes the starting point for the computation of optical tomographic data.

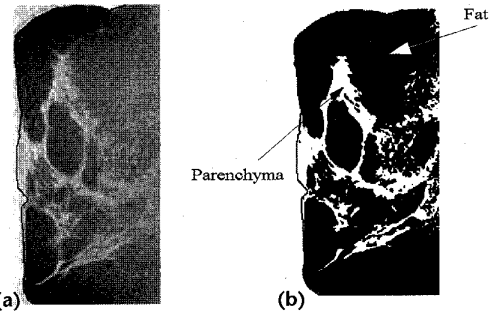

Figure 1. Reference medium: (a) MR-derived sagittal slice of a female breast, (b) the same image after segmenting by tissue type.

Specifically, in the studies conducted here a series of 24 MR images were obtained from the breast of a volunteer using a GE Signa MR system. The fast spin echo (TR = 4000 ms, TE = 112 ms, 3-mm thickness) technique was used, with and without fat and water saturation. Surface coils were used, to obtain better uniformity of the field. Image data were collected with the subject lying prone in the magnet, which caused some degree of dorsal–ventral compression of the breast. Figure 1a shows a sagittal section through one such image. This series of sagittal sections was then used as the reference medium in image reconstructions. Prior to evaluating the MR data for computation of photon intensities, spatial averaging was performed to yield a 3D image of dimension $49 \times 35 \times 24$ voxels.

Each pixel in the digitized MR image had an assigned integer intensity value in the range 1–256. The breast was segmented into two different tissue types—fat and glandular (parenchyma). The segmentation was done by a simple thresholding technique; all MR image pixels with image intensities ≤ 128 were assumed to be fat and all those > 128 were assumed to be parenchyma. We are aware of more accurate segmentation protocols and have adopted these in other studies.[8] Figure 1b shows a sagittal section of a segmented image. Each tissue type was then assigned a set of optical properties—μ_a and μ_s', the absorption and reduced scattering coefficients. Two "pathologies" were introduced by assigning different μ_a and/or μ_s' values to selected voxels in two regions. Figure 2a is a schematic of this. The values in Table 1 identify the range of optical properties assigned to simulate seven different types of tissue backgrounds and added tumors. In all cases except medium IV,

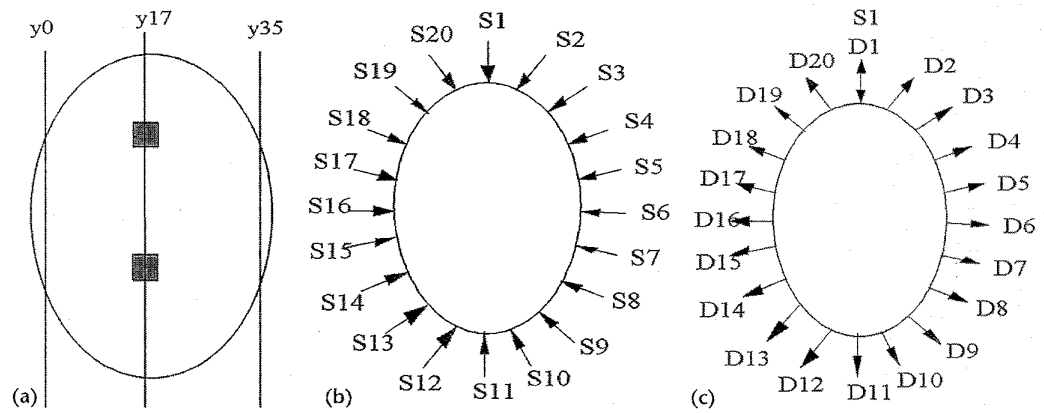

Figure 2. Schematic front (coronal) view of breast showing positions of (a) numbered slices and added "pathologies" (small squares); (b) 20 optical sources; (c) 20 detectors for source S1.

Table 1. Optical coefficients assigned to segmented MR images (in mm^{-1}).

	Fat		Parenchyma		Tumor	
Type	μ_a	μ_s'	μ_a	μ_s'	μ_a	μ_s'
I	0.003	0.20	0.01	0.30	0.05	0.50
II	0.006	0.40	0.02	0.60	0.10	1.00
III	0.012	0.40	0.04	0.60	0.10	1.00
IV	0.012	0.40	0.04	0.60	0.01	0.10
V	0.01	1.00	0.03	0.50	0.50	3.00
VI	0.01	2.00	0.03	1.00	0.50	6.00
VII	0.01	4.00	0.03	2.00	0.50	12.00

the optical coefficients for the "added tumors" exceeded those of the background medium. Taken together, the values chosen cover a range that exceeds the expected values in real tissues at both the high and low ends.

Although in most cases the scattering and absorption coefficients of the pathologies were both perturbed, images were reconstructed according to a model that assumes perturbations only in the absorption coefficients. We use this simplification for three reasons. First, it reduces the computational effort. Second, by reducing the number of unknowns, it should help stabilize computed solutions. Third, and most important, the scattering weight function is generally much smaller than the absorption weight function.

Numerical simulation of optical tomography data

We have evaluated tomographic data sets computed from the seven different background-medium types. Use of a perturbation model requires specification of some type of reference medium. The reference media used here were breast maps lacking the added inclusions. We obtained solutions to Equation 2 using a Jacobi relaxation code. The limitations encountered were mostly due to the computational inefficiency of the Jacobi method. Typical computing times for a single source location were as long as 24 hours on a workstation. As we need 40 such computations (20 reference, 20 test medium) per breast map, the overall computing effort is significant. The effort remained tractable thanks to the availability of multiple workstations at the CASE Center at Syracuse University.

The grid size used for a particular computation varied with the type of optical parameters chosen. In general, we tried to choose grid sizes smaller than the largest value for $\mu_s'^{-1}$. In some cases, due to computational limitations, this was not practical and larger grid sizes were adopted. We are aware that this may lead to some inaccuracies in the computed results, but for the purposes of these computations, such errors should not affect the validity of the reconstruction results. Because different grid sizes were used in the forward problem, the corresponding volume of the breast considered also varied. In effect, we have evaluated a series of breasts that have identical anatomy but are scaled to different sizes. Table 2 shows the specific parameters used to compute solutions to the forward problem for each of the breast types examined. For comparison, results obtained from forward problems having a dimension of $98 \times 70 \times 48$ voxels were then spatially averaged to a grid size of $49 \times 35 \times 24$ before attempting image recovery. The tumor size was also scaled; it measured $6 \times 6 \times 6$ for a large breast and $3 \times 3 \times 3$ for the small.

Any practical system will need more efficient

and flexible numerical solvers than the Jacobi method used here. Two that come to mind are multigrid finite-difference solvers[9] and the finite-element method.[10] Multigrid solvers can greatly increase the speed of convergence over the point Jacobi method we used, but appear to be more cumbersome to implement for media having arbitrary geometries. For this the finite-element method is more appropriate. In either case, computing physically accurate solutions will require careful selection of boundary conditions.[11] It also deserves mention that the appropriateness of applying formulations derived from diffusion theory to evaluation of data from real tissues remains an open question. The concern is whether this approach is sufficiently robust to permit accurate modeling of the range of conditions expected in clinical practice. Should it not be adequate, then more computationally intensive solutions to the transport equation might be required.

A schematic of the tomographic measurement scheme used to simulate data collection is shown in Figures 2b and 2c. In the model, 20 time-independent sources were "placed" at the boundary of the breast and 20 "detector readings" were obtained for each source, for all reference and pathology-containing media. The position of the sources and detector were confined to a coronal plane located halfway between the chest wall and nipple and bisecting the tumors. The normalized photon intensity in each voxel was also recorded for the reference medium in each set for weight matrix calculations.

Image reconstruction

A variety of numerical methods have been developed to solve systems of linear equations. A critical measure of a method's practical usefulness is its performance on ill-conditioned or ill-posed systems. For this problem, there are two principal sources of ill-posedness: factors intrinsic to the model and to the physical measurement. In our case, the weight matrices are invariably ill-conditioned (almost linearly dependent columns). Physically, each column corresponds to a single voxel. As the optical thickness of the medium increases, the weights for neighboring voxels deep in the interior become nearly equal. The weight is a function of, among other things, the source condition; that is, the weight in a particular voxel depends on whether the source is continuous, time-harmonic, or an impulse. Consideration of the trade-offs between cost and complexity of the source condition and the conditioning of the weight matrix is one issue of particular importance. It is also one that can be easily evaluated using the MR-based modeling scheme we have adopted.

Table 2. Parameters used in solving the forward problem.

Type	Problem size (voxels)	Voxel length (mm)	Approx. breast volume (cm^3)	Tumor volume (cm^3)
I	98 × 70 × 48	1.75	1,590	1.16
II	98 × 70 × 48	0.9	215	0.16
III	98 × 70 × 48	0.9	215	0.16
IV	98 × 70 × 48	1.75	1,590	1.16
V	49 × 35 × 24	2.7	730	0.53
VI	49 × 35 × 24	2.7	730	0.53
VII	98 × 70 × 48	1.35	730	0.53

Any real system will have limits on the available views, scan times, source intensities, and number and location of source–detector pairs. Each of these factors also influences the conditioning of the weight matrix. Thus, an important issue to explore will be the dependence of image quality and stability on each of these parameters in relation to practical limits of data collection. Some preliminary results evaluating these issues are described below.

For problems of the type we are considering, selecting an efficient imaging algorithm is a key factor in practical development. Imaging methods that employ forms of energy having well-defined paths through the target (such as X-ray CT) can take advantage of highly efficient transform methods, because of the one-to-one correspondence of each one-dimensional projection in physical space to a one-dimensional contour in Fourier space. Unfortunately, such methods are not applicable to the optical tomography problem. Instead, we have employed the more general, but often computationally more intensive, class of algebraic methods used to iteratively solve systems of linear equations. While many methods are available, selection of which is most appropriate is often based on *a posteriori* evaluation of the image quality and algorithm stability. In our studies we have selected three algorithms, all basically algebraic solvers. Two of these, the conjugate gradient descent (CGD) and simultaneous algebraic reconstruction technique (SART), are simultaneous methods, while the third, projection onto convex sets (POCS), is sequential.

In the CGD method,[12] all data from detector readings are incorporated into each update at the same time. The formula for the estimate of $\Delta\mu_a$ in the nth iteration, $\Delta\mu_a^n$, is

$$\Delta\mu_a^n = \Delta\mu_a^{n-1} - \alpha^n \mathbf{d}^n \qquad (9)$$

where

$$\alpha^n = \frac{\left\|\mathbf{g}^{n-1}\right\|^2}{\left\|W\mathbf{d}^n\right\|^2}, \quad \mathbf{d}^n = -\mathbf{g}^{n-1} + \beta^n \mathbf{d}^{n-1},$$

and

$$\beta^n = \frac{\left\|\mathbf{g}^{n-1}\right\|^2}{\left\|\mathbf{g}^{n-2}\right\|^2}, \quad \mathbf{g}^{n-1} = W^{\mathrm{T}}\left(W\Delta\boldsymbol{\mu}_a^{n-1} - \Delta\mathbf{R}\right)$$

The initial estimate of the absorption coefficient perturbation is $\Delta\boldsymbol{\mu}_a^0$, and the initial values taken for the other parameters[12] are $\mathbf{g}^0 = W^{\mathrm{T}}(W\Delta\boldsymbol{\mu}_a^0 - \Delta\mathbf{R})$, $\beta^1 = 0$, and $\mathbf{d}^1 = -\mathbf{g}^0$. The gradient and conjugate gradient vectors are denoted by $\mathbf{g}^n$ and $\mathbf{d}^n$, respectively, α^n is the step size, and $\|\cdot\|$ denotes the Euclidean norm of a vector. Theoretically, this algorithm should converge after a number of iterations less than or equal to the number of unknowns. In practice, round-off errors in the computations may increase the number of iterations required for convergence, or prevent it altogether.

The ART (algebraic reconstruction technique) method was first developed in the early 1970s for reconstructing 3D images of cell organelles from sets of 2D electron micrographs. It has since been widely used as a reconstruction algorithm for X-ray CT and has undergone many revisions.[13] ART is a sequential algorithm and the images it produces typically exhibit certain characteristic types of artifacts. A simultaneous algorithm named SIRT (simultaneous iterative reconstruction technique) was developed in part as a remedy for these artifacts, but it tends to converge more slowly than ART.[13] The SART algorithm combines the positive features of ART and SIRT. The formula used to compute the nth estimate of the absorption perturbation in the jth voxel is[13]

$$\Delta\mu_{a,j}^n = \Delta\mu_{a,j}^{n-1} + \frac{\sum_i w_{ij} \dfrac{\Delta R_i - \sum_{j'} w_{ij'} \Delta\mu_{a,j'}^{n-1}}{\sum_{j'} w_{ij'}}}{\sum_i w_{ij}} \tag{10}$$

where i is the source–detector pair index. We chose the SART algorithm because of its tendency to enhance image features in regions where all the w_{ij} are small.

POCS is a sequential projection method that reaches the intersection point of L constraint sets by projecting the current estimate of the solution onto each set C_l (a set which satisfies the lth constraint), $l = 1, 2, \ldots, L$, sequentially and iteratively.[12] A set is convex if any linear combination $kx + (1 - k)y$ of two of its elements x and y, with $0 < k < 1$, is also a member of the set. Lines, circles, and squares, and their higher-dimensional analogs, are familiar examples of convex sets. Each step in POCS can be represented by

$$\Delta\boldsymbol{\mu}_a^n = P_L \circ P_{L-1} \circ \ldots \circ P_1 \Delta\boldsymbol{\mu}_a^{n-1} \tag{11}$$

Here, P_l represents the projection operator onto C_l, such that $P_l \Delta\boldsymbol{\mu}_a^n$ is the element in C_l that is closest to $\Delta\boldsymbol{\mu}_a^n$, and the symbol $\circ$ denotes composition of functions. It has been proved that, as long as the intersection of the constraint sets is not empty, iterative projections onto these sets will converge to their intersection.[12] The subspace of solutions to each linear equation in Equation 8 is a convex set. An advantage of POCS is that it can easily incorporate nonlinear constraints in addition, if the sets of solutions to those constraints are convex. The usual source for these nonlinear constraints is a priori information, that is, known properties of the medium that help limit the set of possible solutions. An example would be a range constraint, which limits the values of the reconstructed results.

Computational issues should also be considered, such as how well a specified reconstruction algorithm can be mapped to the architecture of a particular computing platform. Further, factors influencing which algorithm is most appropriate will themselves be functions of such things as limitations of measurement and properties of the target medium. For this reason, we believe that we must continue to consider more than one algorithm.

Results of optical imaging experiments

In the following, we describe the results we obtained based on the analysis of MR-derived segmented maps. Results presented amount to a first-order Born solution. Recently, we have extended this to include a recursive solver where the initial solution is used to update the forward problem and where both the diffusion and absorption coefficient perturbations are solved for simultaneously.[8] In all cases, we performed 2D reconstructions (forcing the image to be symmetric in the direction perpendicular to the plane defined by the sources and detectors) and we imposed positive range constraints on reconstruction results after each iteration: $\Delta\mu_{a,j}^n = 0$ if $\Delta\mu_{a,j}^n < 0$. Also, in all cases, computed images were based on analysis of underdetermined data sets (that is, 400 source–detector pairs, 1,584 unknowns (the num-

ber of voxels in the reconstructed image)). For reconstructions with added noise, a number sampled from a Gaussian pseudorandom number generator was added to each computed detector reading. Noise is quantified by means of the signal-to-noise ratio, which we define as

$$\text{SNR} = 10 \log_{10} \frac{\text{average signal power}}{\text{noise variance}} \quad [\text{in dB}] \tag{12}$$

Figure 3 shows a plot of the logarithm of computed photon intensities in several sagittal views for a source directed normal to the breast in the region of the nipple (left side). The particular case is based on Type V background conditions. Figure 3a shows the result for the reference medium without added tumors, and 3b the result when two tumors are added. The two darkened structures in slice y17 indicate the position of the added tumors. The jagged edge on the left illustrates the detected edge of the tissue for the particular thresholding values chosen and does not represent an error in solving the forward problem.

Data shown in Figure 4 are the computed detector responses for each of the background conditions tested for a source located at position 6. Inspection reveals that, as expected, a large range of intensity values is obtained, with the detector located opposite the source (refer back to Figure 2) usually having the lowest values. Comparison of these values to allowable source intensities indicates that only the Type VII medium yields values that are so low as to be effectively unmeasurable. Background scattering properties for Types V and VI media are within the range reported for breast tissue. The others represent values that likely underestimate the transport scattering lengths. As indicated in Table 2, the physical dimensions of the former correspond to a breast volume of approximately 730 cm^3, which, at the position of the sensor array, is equivalent to probing a tissue thickness of approximately 10 cm. We consider this finding encouraging, as it suggests that physical measurements could be performed on breasts of this size and still yield useful data without the usual rostral–caudal compression used in X-ray mammography.

Figure 5 shows the results of 2D reconstructions using the CGD algorithm for each of the different test media containing added tumors, after 1,000 iterations. In all cases, both tumors are well resolved, their locations are correctly identified, and the image is relatively free of artifacts. What qualitative errors are observed are mainly due to an underestimate in the physical sizes of the tumors, which appears most pronounced for

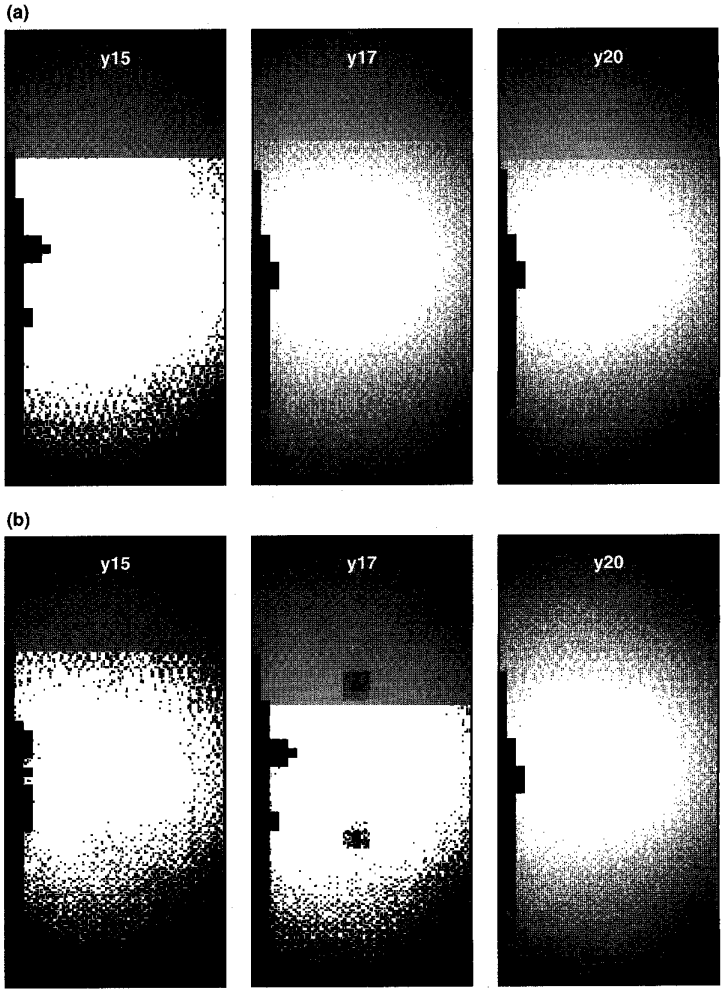

Figure 3. Computed solutions to the forward problem (time-independent diffusion equation) illustrating diffuse intensities inside the breast model based on real MR-derived geometry. (a) the reference breast medium, (b) medium containing two simulated "pathologies." Note the added "tumors" in slice y17.

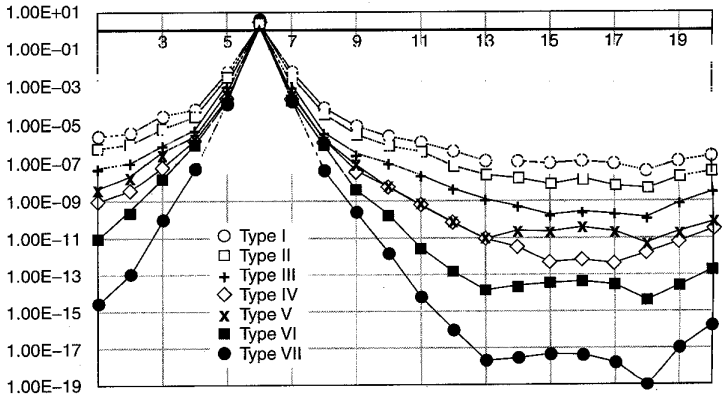

Figure 4. Computed surface intensity values for source position 6, for the different assigned values of optical coefficients listed in Table 1. Values shown correspond to simulations in the presence of added "pathologies." The *y* axis is the log of the detected intensity.

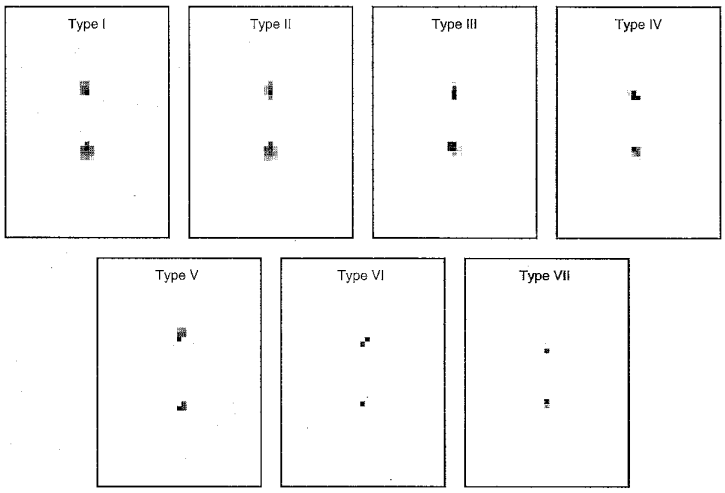

Figure 5. Reconstructed images of MR-segmented data sets with added tumors, showing the promise of optical tomography.

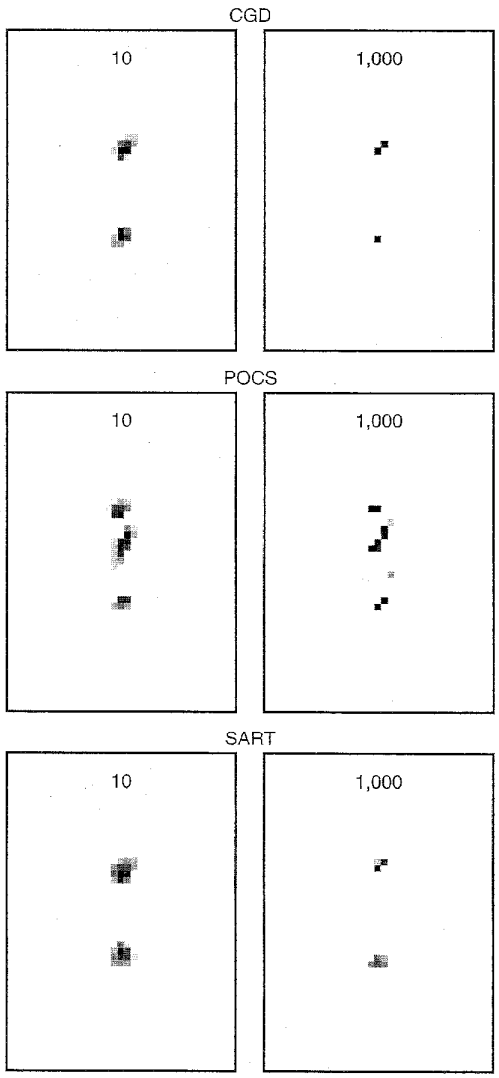

Figure 6. Images obtained of Type VI media using the CGD, POCS, and SART algorithms, with no added noise, after the indicated number of iterations.

tissue backgrounds having the largest values of reduced scattering coefficients. It is not surprising that less-than-perfect images are recovered, given that the computed solutions correspond to a single step of the perturbation model. A comparison of image quality achieved using the different algorithms as a function of iteration number is shown in Figure 6 for the Type VI medium. Results show similar image quality is obtained using the CGD and SART algorithms and that good separation is achieved after only 10 iterations. For these data sets, results from the POCS algorithm were of poorer quality, with artifacts in the central region. Because the order in which the data are analyzed can influence the computed result, additional testing of the POCS algorithm is necessary before conclusions can be made regarding its suitability to this problem.

Adding noise

As any real measurement contains noise, it is important to examine the stability of computed solutions to added noise in the detector readings. Results shown in Figure 7 are reconstructions obtained after 100 iterations with the SART algorithm when 0 dB Gaussian white noise was added to the noise-free detector readings. (This is a lot of noise—a level equal to the mean value of the signal strength; see Equation 12.) Inspection reveals that the influence of noise is strongly dependent on the type of background medium. In fact, rather paradoxically, it appears to be negatively correlated with the background scattering coefficient (that is, the stronger the background scattering, the *less* effect noise has on the image). For Type I media, the computed image is mostly artifact. For Types II and III, the images of the two tumors coalesce into a single central mass. For Type IV media, the two tumors are evident but their image densities are not the same. For the other types, good separation of the tumors is evident. Interestingly, however, even for Type I media, a qualitatively accurate solution can be achieved by simply increasing the number of iterations; in the case shown, to 3,000.

It deserves mention that the level of added noise is greater than would ordinarily be expected to yield usable images. While usually this finding would be very positive, our enthusiasm is tempered by the observation that because the range of the detector readings spans many orders of magnitude, the added noise primarily affects the lowest detector readings. In addition, we have imposed range constraints on the reconstruction results and limited the dimensions of the unknowns to only a single coefficient. In practice, because differences in scattering will cause a redistribu-

tion of photons, the ability to compute quantitatively accurate solutions will require that less stringent range constraints be imposed and that solutions for both absorption and scattering be attempted. Reconstruction of both will be necessary in order to implement algorithms in which iterative updates of the forward problem are computed. In fact, we have recently reported preliminary findings obtained from MR breast maps in which both coefficients were simultaneously solved for without imposition of any range constraints. In that work we observed a much greater sensitivity to added noise.[8]

Other sources of error

For an arbitrary medium, there are basically four sources of error in specifying the reference state: incorrect estimates of its overall shape, its volume, its internal structure, or its assigned coefficients. Should MR data be available, especially if they were acquired simultaneously with the optical measurement, then specification of the first three should be fairly straightforward. As for the last, specification of the optical coefficients ideally should come from the measured optical data. This is a nontrivial issue that has received inadequate attention. In principle, errors in estimates of the reference could be compensated for by performing iterative updates of the forward problem. This might be feasible, should only a few updates be required. However, if a large number are needed, the computational burden could quickly become unmanageable, especially for 3D problems. Should any reader have practical insights into this, the authors would be most grateful in learning about them.

Results shown in Figures 8 and 9 examine the effect that errors arising from three of the above-mentioned sources have on image quality, as a function of algorithm used. We assume accurate knowledge of the shape of the medium, but introduce systematic errors in the other factors. Our motivation for undertaking this study is an appreciation that, in practice, knowledge of the correct reference medium, from which the weight functions are calculated, is itself incomplete. Thus, it is likely that only an approximation can be made. For the results shown in these figures, we have modeled the effects of inaccurate estimates of the background scattering coefficients, of assuming the reference medium is homogeneous, and of over/underestimating the breast size. For the first computation, we used weight functions derived from the Type V medium to evaluate the detector readings from the Type VI medium, and vice versa. Table 1 shows that these media differ only in the values of the assigned scattering coefficients. In this case we assume accurate knowledge of the anatomy (breast shape, volume, and internal structure) but not of the optical coefficients. Figure 8 shows that, except for images computed using the POCS algorithm, surprisingly good reconstructions are obtained. Also shown in Figure 8 is the effect of the case in which the reference medium is assumed to be homogeneous. In this case only artifacts are reconstructed. It would appear, therefore, that some knowledge of the internal composition is required to recover a qualitatively accurate image, at least for a one-step solution of the perturbation model.

To study the effect of errors in the estimated volume, we conducted a study similar to the preceding, but interchanging weight functions and detector readings for Types III and IV media. These media have the same background optical coefficients but differ in volume by a factor of eight. Thus, we assume accurate knowledge of the internal structure, overall shape, and coefficients. Figure 9 shows, interestingly, that errors in assumed volume lead to errors in the distance between the

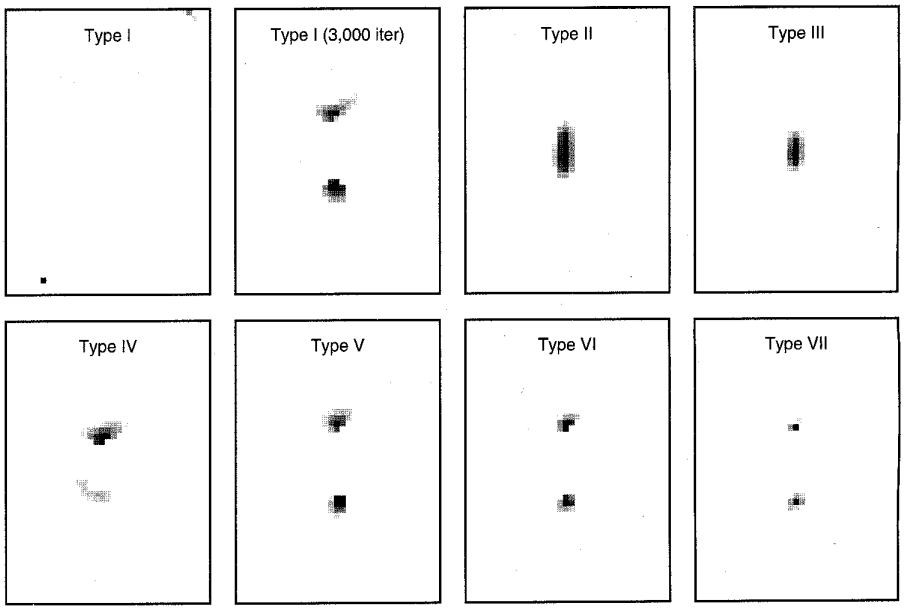

Figure 7. Images after 100 iterations (and in one case, 3,000) with the SART algorithm in the presence of considerable added noise.

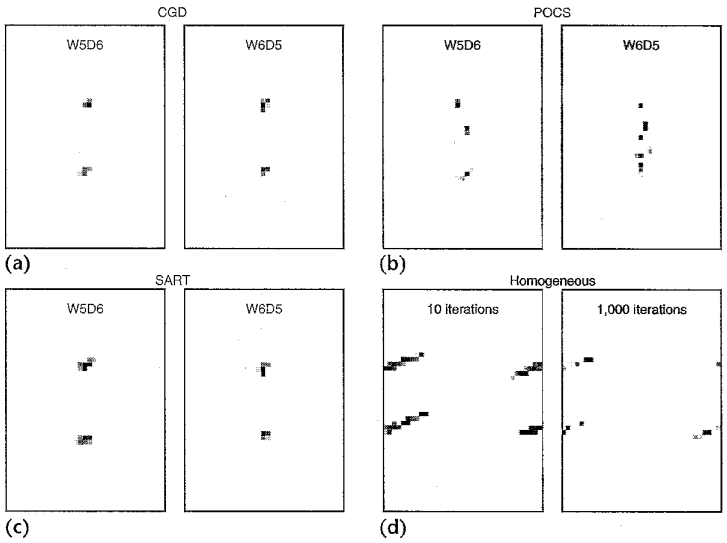

Figure 8. Analysis of sources of error. (a)–(c) Images for Types V and VI media calculated with wrong weights, using the CGD, POCS, and SART algorithms in the absence of added noise after 1,000 iterations. W5D6 means the weight function computed for Type V media was used to evaluate detector readings from Type VI media. W6D5 means the opposite. (d) Assuming a homogeneous reference medium, after 10 and 1,000 iterations.

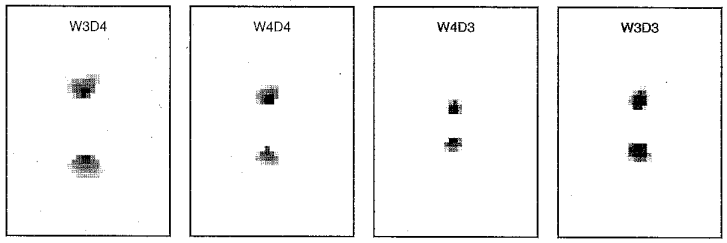

Figure 9. Analysis of sources of error. Images obtained using the SART algorithm after 100 iterations, for Type III and IV media. For abbreviation scheme see Figure 8.

Table 3. Quantitative comparison of reconstruction results (CGD algorithm, noise-free data, 1,000 iterations). Columns list values for upper and lower virtual "tumors."

Medium type	True $\Delta\mu_a$ (mm^{-1})	Computed $\Delta\mu_a$ (mm^{-1})	
		Upper	Lower
I	0.24	0.076	0.096
II	0.48	0.14	0.18
III	0.46	0.14	0.28
IV	−0.53	1.05	0.51
V	2.47	0.32	0.24
VI	5.47	0.48	0.37
VII	10.47	0.60	1.97
W5D6	5.47	0.0013	0.0010
W6D5	2.47	122	78

reconstructed tumors, the direction of which depends on the source of the weight function.

Thus far, results shown have emphasized the qualitative accuracy and stability of computed images. A quantitative analysis of the image data obtained by the CGD algorithm for the different breast types is shown in Table 3. These results are derived from data shown in Figure 5. The tabulated numbers correspond to the integrated image intensity values for the virtual tumors present in the upper and lower halves of the images. Also listed are some corresponding values when an incorrect weight function is used. Three interesting observations can be made. First, even though qualitatively accurate results can be obtained, there are significant quantitative errors. Second, the magnitude of this error increases with increases in the strength of the perturbation. Third, a two-fold systematic error in the weighting functions can produce large quantitative errors (approximately 300-fold) in the estimated cross-section perturbations. These findings strongly suggest that to recover quantitatively accurate results, it will be necessary to compute iterative updates to the forward and inverse problems.

Next we turn to issues regarding data collection. As mentioned, variables under experimental control include, among others, the source condition, number and location of sources, and number and location of detectors per source. For the results included in this article, all simulated detector values were obtained using time-independent sources. (The reader is referred elsewhere[8] for preliminary results on similar studies using time-harmonic sources.) Figures 10 and 11 show results of our examination of the effect of limiting the view angle of measurement in the forward, backward, and side directions, and the effect of a uniform but sparse detector scheme.

Figure 10 illustrates the variables we examined. Figure 10a shows the geometry of measurement when three detectors in the forward (side opposite each source) hemisphere are deleted (darkened circles). Figure 10b shows the configuration for a uniform but sparse detection. Figures 10c illustrates a configuration complementary to that in 10a (that is, detectors are deleted in the backward hemisphere). Figure 10d models a compressed geometry (no sources or detectors at the sides). For clarity, we adopt the abbreviations xS for number of sources, xD for number of detectors per source, and the subscripts f for forward and b for backward.

Results of this study, using the SART algorithm for a range of different geometries of measurement, are shown in Figure 11. The image labeled 20S–20D is the control (no detectors or sources

deleted). The effect of implementing a sparse configuration is shown in the next two panels (20S–10D and 10S–10D). Halving the number of detectors per source causes a significant distortion in the image, but the tumors still are successfully resolved. If the number of sources is also halved (to 100 source–detector pairs), only artifact is recovered. The next image to the right shows the effect of deleting sources and detectors from the sides, the so-called compressed geometry. Interestingly, the effect is qualitatively similar to that seen for the case of 20S–10D sparse geometry. The middle three panels show the effect of deleting three, five, and seven adjacent detectors in the forward hemisphere. The bottom four panels show the effect of deleting three to nine adjacent detectors in the backward hemisphere. Qualitatively, the results are roughly equivalent; deleting more detectors produces images in which tumor locations are increasingly inaccurate, the distance separating tumors is increasingly underestimated, and the level of artifacts is greater.

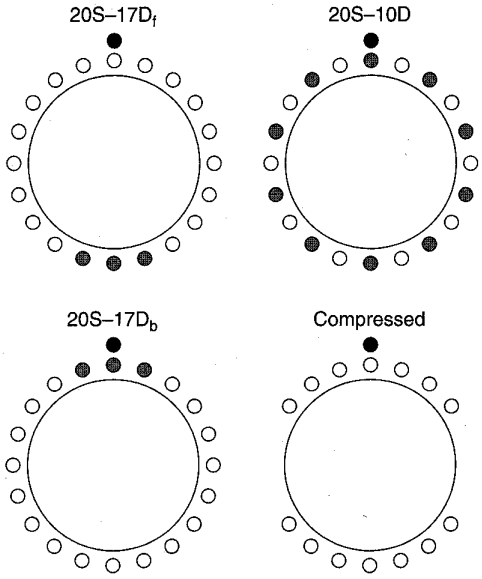

Figure 10. Source–detector geometries used for view-angle study.

When the same data were evaluated using the CGD algorithm (not shown), qualitatively similar results were obtained but with an even greater artifact level. A quantitative comparison of images reconstructed with added noise revealed that while qualitatively recognizable images were obtained, the computed cross sections are strongly influenced by added noise. The magnitude and direction of this effect varies with the number and geometric arrangement of sources and detectors.

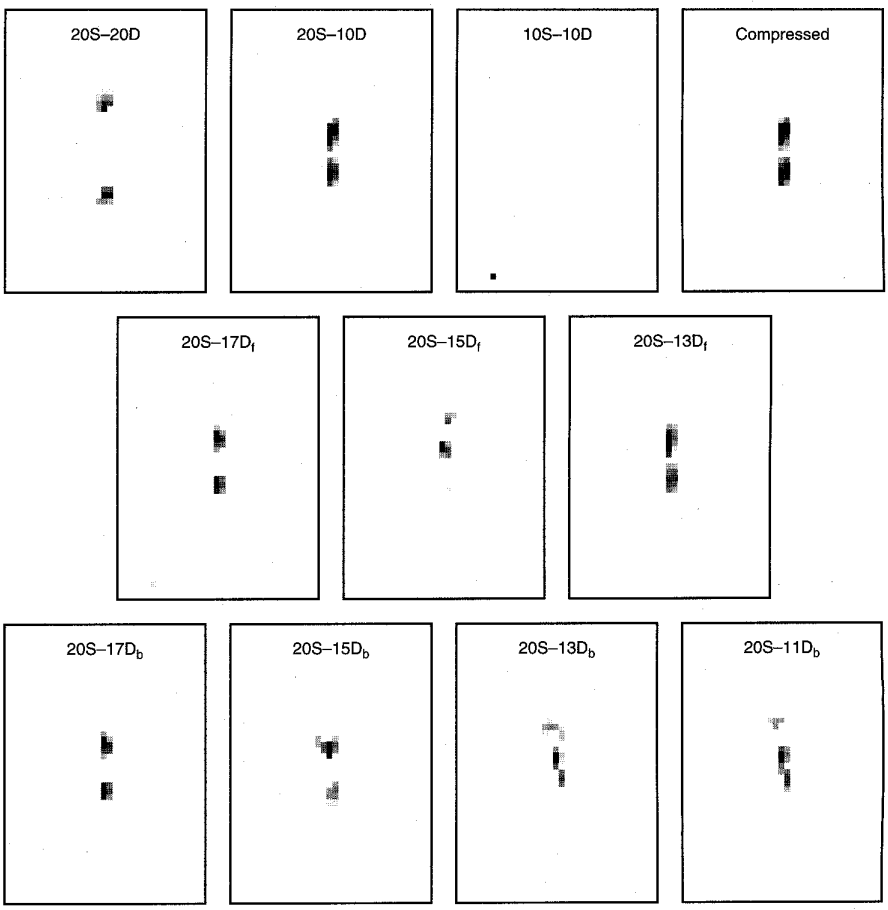

Figure 11. More analysis of sources of error: effects of varying the number of optical sources and detectors. Images were obtained using the SART algorithm after 1,000 iterations for a Type V medium. The indicated illumination geometries are explained in Figure 10 and in the text.

We have examined the potential utility of incorporating MR-derived anatomical image data to aid in the computation of tomographic images of the female breast based on the analysis of computed time-independent near-infrared optical measurements. There are some, especially among those who serve on study sections of the National Institutes of Health, who discount the feasibility of imaging thick tissues at NIR

wavelengths. Whereas we recognize that many of the computations reported assume detailed prior knowledge about the target medium, it is our belief that if the MR data are obtained at the same time as the optical data, this assumption can be largely satisfied. We also realize that even if such knowledge is available, there is much still to be learned and tested before practical systems can be developed. Examples of outstanding questions are

- Given the expected range of pathologies that exist in clinical settings, is the diffusion approximation an adequate modeling scheme or will more computationally intensive solutions to the transport equation prove necessary?
- Are solutions to the first-order Born or Rytov approximations sufficient, or will iterative updates be required?
- Is a perturbation formulation computationally tractable for 3D imaging?
- Can a free-standing imaging system be developed?

We contend that the ability to answer such questions will be greatly facilitated by evaluating anatomically accurate models such as those easily derived from MR data. Much work remains, with no guarantee of success. We do hope, however, that the results presented here put to rest any doubts regarding the intrinsic feasibility of computing tomographic images based on the analysis of diffusely scattered light. While these results are preliminary, we believe they strongly suggest that the problem is solvable. No doubt this technique is computationally much more intensive than X-ray CT or MR imaging. However, significant improvements in computational speed occur regularly. What remains is to work out the details. To those who ask "why bother?," we remind the reader that optical methods are orders of magnitude more sensitive than other imaging modalities, that they are capable of monitoring situations and events critical to sustaining life, that they employ nondamaging energy sources, and that the instrumentation can be relatively compact, portable, and low in cost.

Specific insights gained from the current studies point to the importance of having prior knowledge of the internal anatomy and of using fully tomographic data collection schemes. A point of further study will be to ascertain the sensitivity of image quality to errors in image segmentation. In particular, it should be useful to demonstrate whether MR data "averaged" for a defined parameter set (breast size, age, skin color, etc.) over some subset of the adult female population can be substituted for MR data on a specific individual.

Finally, it deserves mention that there are at least two additional measurement parameters, spectroscopic data and fluorescence, that are yet to be fully explored and that could aid in the optical tomography problem. Fluorescence is appealing because, like MRI but unlike radioisotopes, it is often sensitive to changes in the immediate chemical environment. Fluorescent probes have been successfully substituted for radioisotopes in many *in vitro* diagnostic methods. Their use in tomographic imaging applications would be a natural extension. Computationally, fluorescence tomography requires the solution of two coupled inverse problems. The first deals with the problem described here. This is necessary to predict the distribution of the excitatory field. The second computes the distribution of fluorescence parameters from measurements of fluorescent light emerging at the surface. Through judicious selection of fluorescence probes that are sensitive to chemical environments often associated with diseased states and by linkage of these to specific biotargeting agents, such as a monoclonal antibody, significant increases in the sensitivity and specificity of diagnostic procedures might be achieved. ◆

Acknowledgments

This work was supported in part by NIH grant R01 CA59955, by ONR grant 0014510063, and by the New York State Science and Technology Foundation.

References

1. M. Cutler, "Transillumination as an Aid in the Diagnosis of Breast Lesions," *Surgery, Gynecology and Obstetrics*, Vol. 48, 1929, pp. 721–729.
2. A. Ishimaru, *Wave Propagation and Scattering in Random Media*, Vol. 2, Academic Press, New York, 1978, Ch. 15.
3. R. Aronson et al., "Application of Transport Theory to Infra-Red Medical Imaging," in *Modern Mathematical Models in Transport Theory: Advances and Applications*, Birkhäuser Verlag, Basel, Switzerland, 1991, pp. 64–75.
4. R.L. Barbour et al., "Model for 3-D Optical Imaging of Tissue," *Remote Sensing Science for the Nineties: Proc. 10th Ann. Int'l Geoscience & Remote Sensing Symp. [IGARSS '90]*, IEEE Press, New York, 1990, pp. 1,395–1,399.
5. J.R. Singer et al., "Image Reconstruction of the Interior of Bodies that Diffuse Radiation," *Science*, Vol. 248, 1990, pp. 990–993.
6. S.R. Arridge et al., "New Results for the Development of Infra-Red Absorption Imaging," *Proc. Biomedical Image Processing*, SPIE Proceedings Vol. 1245, SPIE, Bellingham, Wash., 1990, pp. 92–103.
7. J. Chang et al., "Recovery of Optical Cross Section Perturbations in Dense Scattering Media Using Transport-Theory-Based Imaging Operators and Steady-State Simulated Data," to be published in *Applied Optics*.
8. Y. Yao et al., "Frequency Domain Optical Tomography in Human Tissue," *Proc. Experimental and Numerical Methods for Solving Ill-Posed Inverse Problems: Medical and Nonmedical Applications*, SPIE Proceedings Vol. 2570, SPIE, Bellingham, Wash., Oct. 1995.
9. A. Brandt, "Multi-Level Adaptive Solutions to Boundary-Value Problems," *Mathematics of Computation*, Vol. 31, No. 138, 1977, pp. 333–390.
10. G. Strang and G.J. Fix, *An Analysis of the Finite Element Method*, Prentice Hall, Englewood Cliffs, N.J., 1973, Ch. 7.

11. R. Aronson, "Boundary Conditions for Diffusion of Light," *J. Optical Soc. Am. A*, Vol. 12, 1995, pp. 2,532–2,539.
12. H. Stark, ed., *Image Recovery: Theory and Application*, Academic Press, San Diego, Calif., 1987.
13. A.C. Kak and M. Slaney, *Principles of Computerized Tomographic Imaging*, IEEE Press, New York, 1988, Ch. 7.

Randall L. Barbour is associate professor of pathology and biophysics and director of clinical chemistry at the State University of New York Health Science Center at Brooklyn. He earned his PhD in biochemistry from Syracuse University in 1981, and has written numerous papers on methods for imaging in random media and on the application of noninvasive methods for the study of organ function. Barbour is a member of IEEE, the American Association for Clinical Chemistry, and FASEB. He is active in SPIE, and has recently chaired conferences on medical imaging and numerical methods for solving ill-posed inverse problems. He also serves on NIH study sections for diagnostic imaging and lasers and spectroscopy.

Harry L. Graber earned his AB with a concentration in chemistry from Washington University in 1983, and will receive a PhD from the Program in Physiology and Biophysics of the SUNY Health Science Center at Brooklyn in 1996. His research interests include biomedical optics, medical imaging, and medical physics. Graber is a member of the Biophysical Society, the IEEE, and the Optical Society of America.

Jenghwa Chang earned his BS and MS from the Department of Control Engineering and the Institute of Communication Engineering, National Chiao-Tung University, Taiwan, and his PhD in electrical engineering from Polytechnic University of New York in 1994. He is a research assistant professor at the Department of Pathology, SUNY Health Science Center at Brooklyn. His research interests include medical imaging, signal and imaging processing, electromagnetics, medical physics, and biomedical optics.

San-Lian Susan Barbour holds a postgraduate electrical engineering degree from Syracuse University, an MS in physics from Sam Houston State University, and a BS in physics from National Central University, Taiwan. She has worked in electromagnetic field analysis and synthesis, numerical methods, and hardware design; is currently director of software engineering at Bioimaging Sciences Corp., West Orange, N.J.; and is also a member of the technical staff at AT&T Bell Laboratories. She is a member of the IEEE Antennas and Propagation Society and the IEEE Biomedical Engineering Society.

Ping Chen Koo received his PhD in computer and information science from Syracuse University in 1993. His research interests are in parallel processing and the application of efficient numerical methods for solving radiation transport problems. He currently serves as an independent consultant to Bioimaging Sciences Corp. and to the SUNY Health Science Center at Brooklyn. He is a member of the IEEE Computer Society.

Raphael Aronson has been president of Bioimaging Sciences Corp. since 1993. For the prior 20 years he was professor of physics at Polytechnic University, Brooklyn, N.Y. He earned his PhD in physics from Harvard in 1951. A nationally recognized expert in transport theory, Monte Carlo simulation codes, and the modeling of photon transport in tissue, Aronson was a pioneer in the study of deep penetration of neutrons and photons. He was responsible for much early work in reactor shielding. He developed the transfer matrix method in transport theory and has applied it to both neutron penetration and to radiative transfer in terrestrial and planetary atmospheres. Aronson serves on the editorial board of *Transport Theory and Statistical Physics*.

The authors can be reached in care of Randall L. Barbour, SUNY Health Science Center at Brooklyn, 450 Clarkson Ave., Box 25, Brooklyn, NY 11203; e-mail, barbour@sacc.hscbklyn.edu.